

Oscillating magnetoresistance in graphene p - n junctions at intermediate magnetic fields

Hiske Overweg, Hannah Eggimann, Anastasia Varlet, Marius Eich,
Pauline Simonet, Yongjin Lee, Klaus Ensslin, and Thomas Ihn
Solid State Physics Laboratory, ETH Zürich, CH-8093 Zürich, Switzerland

Ming-Hao Liu and Klaus Richter
Institut für Theoretische Physik, Universität Regensburg, D-93040 Regensburg, Germany

Kenji Watanabe and Takashi Taniguchi
Advanced Materials Laboratory, National Institute for Material Science, 1-1 Namiki, Tsukuba 305-0044, Japan

Vladimir I. Fal'ko
National Graphene Institute, University of Manchester, Manchester M13 9PL, UK
(Dated: December 23, 2016)

We report on the observation of magnetoresistance oscillations in graphene p - n junctions. The oscillations have been observed for six samples, consisting of single-layer and bilayer graphene, and persist up to temperatures of 30 K, where standard Shubnikov-de Haas oscillations are no longer discernible. We explain this phenomenon by the modulated densities of states in the n - and p -regions. A periodicity corresponding to a filling factor difference of 8 hints at a selection rule governing transitions between even and odd symmetry Landau levels.

The possibility to combine electron- and hole-like transport has led to the observation of a variety of interesting phenomena in graphene p - n junctions. In the absence of a magnetic field p - n junctions can give rise to Fabry-Pérot oscillations¹⁻³, for which the oscillation period depends on the length of the cavity. In the presence of an external magnetic field B perpendicular to the graphene plane this effect disappears when the cyclotron diameter becomes smaller than the characteristic length of the cavity. At low magnetic fields, in the range of $B = 50$ mT up to $B = 2$ T, depending on sample size and quality, snake states^{4,5} have been observed. Their periodicity is dictated by the length of the p - n interface. In the quantum Hall regime the (partial) equilibration of edge channels⁶⁻¹⁰ and their shot noise^{11,12} have been studied.

We explore yet another phenomenon in graphene p - n junctions, in the magnetic field range below the onset of the quantum Hall effect. We observe magnetoresistance oscillations persisting up to temperatures as high as 30 K and occurring over a large density range. The oscillatory pattern is the same for samples with one and two p - n interfaces, monolayer and bilayer graphene, interface lengths ranging from $1 \mu\text{m}$ to $3 \mu\text{m}$ and is essentially particle-hole symmetric. The oscillations have been observed in a magnetic field range of $B = 0.4$ T up to $B = 1.4$ T. Their periodicity does not match the periodicity of the aforementioned snake states. In this paper we address this phenomenon and suggest a model which can quantitatively explain the oscillations.

Measurements were performed on six samples in total, which all consist of a graphene flake encapsulated between two hexagonal boron nitride (h-BN) flakes on a Si/SiO₂ substrate. They all show similar behavior. This

sample name	A	B	C	D	E	F
sample width W (μm)	1.3	1.4	1.1	0.9	3	1.2
sample length L (μm)	3.0	1.4	1.0	2.3	3	2.8
top gate length L_{TG} (μm)	1.1	0.7	0.55	1.2	1.0	1.0
distance to top gate (nm)	23	44	28	57	35	25
number of graphene layers	2	1	2	2	2	2
junction type	npn	pn	npn	pn	npn	npn

TABLE I. Characteristics of samples A-F

paper focuses on measurements performed on one sample (sample A), with the device geometry sketched in Fig. 1a. Specifications of the other five samples are summarized in table I. The bilayer graphene (BLG) flake was encapsulated with the dry transfer technique described in Ref. 13. A top gate was evaporated on the middle part of the sample, which divides the device into two outer regions, only gated by the back gate (single-gated regions), and the dual-gated middle region. The other five samples were made with the more recent van der Waals pick-up technique.¹⁴ Unless stated otherwise, the measurements were performed at 1.7 K. A constant voltage bias was applied symmetrically between the Ohmic contacts ('source' and 'drain' in Fig. 1a, inner contacts in Fig. 1b) and the current between the same contacts was measured. The transconductance dG/dV_{TG} was measured by applying an AC modulation voltage to the top gate.

Figure 1c shows the conductance as a function of top gate voltage V_{TG} and back gate voltage V_{BG} . Charge neutrality of the single-gated regions shows up as a horizontal line of low conductance and is marked by a white line. The diagonal line of low conductance corresponds

to charge neutrality of the dual-gated region. The slope of this line is given by the capacitance ratio of the top and back gate. Together these lines divide the map into four regions with different combinations of carrier types: two with the same polarities in the single- and dual-gated regions (pp' and nn') and two with different polarities (nnp and pnp). The conductance in the latter regions shows a modulation which is more clearly visible in the transconductance (see Fig. 2a). The oscillatory conductance is caused by Fabry-Pérot interference of charge carriers travelling back and forth in the region of the sample underneath the top gate. Their periodicity yields a cavity length $L_{TG} = 1.1 \mu\text{m}$, which is in agreement with the lithographic length of the top gate. The Fabry-Pérot oscillations were studied in more detail in Ref. 3, which revealed the ballistic nature of transport in the dual-gated region.

The Fabry-Pérot oscillations disappear in a magnetic field of $B \gtrsim 100 \text{ mT}$ (see Fig. 2b-d). Yet at magnetic fields of $B = 0.4 \text{ T}$ a new oscillatory pattern appears in the nnp and pnp regime. This can be seen in the conductance and transconductance maps recorded at $B = 0.5 \text{ T}$, shown in Figs. 3a,b,d,e. The oscillations follow neither the horizontal slope of features taking place in the single-gated region, nor the diagonal slope of the dual-gated region. They are therefore expected to occur at the interface between the p - and n -doped regions. This was confirmed by measurements on sample D, which had two contacts in the single-gated region and two contacts in the dual-gated region. For this sample, only the conductance along paths involving the interface shows oscillations.

On top of this novel oscillatory pattern the transconductance of sample A in Fig. 3b(e) shows faint diagonal lines in the $nn'n(pp'p)$ regime, which are Shubnikov-de Haas oscillations in the dual-gated region. The occurrence of Shubnikov-de Haas oscillations shows that in this moderate magnetic field regime the Landau levels are broadened by disorder on the scale of their spacing, resulting in a modulation of the density of states.

Using a plate capacitor model described in the supplemental material of Ref. 3, the gate voltage axes can be converted into density and filling factor axes, ν_X with $X = \text{SG, DG}$ for the single- and dual-gated regions, respectively. The result of this transformation is shown in Fig. 3c. The oscillatory pattern has a slope of one, i.e. it follows lines of constant filling factor difference $\Delta\nu = \nu_{\text{SG}} - \nu_{\text{DG}}$. It appears that the oscillations can be described by:

$$G = \langle G \rangle + A \cos\left(2\pi \frac{\Delta\nu}{8}\right) \quad (1)$$

where A is the amplitude of the oscillations, which is on the order of 4 % of the background conductance $\langle G \rangle$ at $T = 1.7 \text{ K}$. The distance between one conductance maximum and the next can therefore be bridged by either changing the filling factor in one region by 8, or by changing the filling factor in both regions by 4 oppositely.

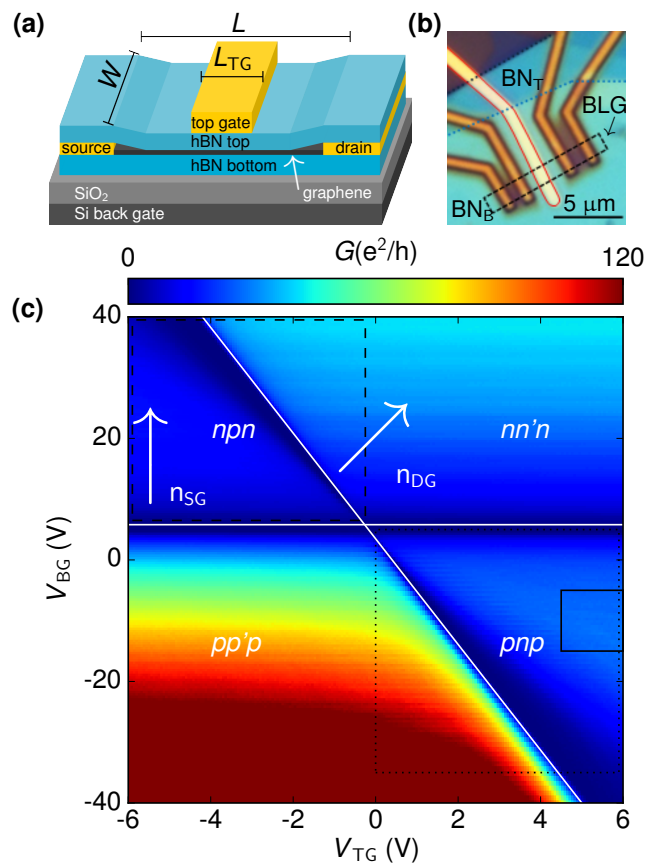


FIG. 1. Characterization of the device. (a) Schematic of the device: a bilayer graphene flake is encapsulated between hBN layers. It is contacted by Au contacts and a Au top gate is patterned on top, which defines the dual-gated region. (b) Optical microscope image of the sample. The four contacts, of which only the inner ones were used, appear orange. The top gate is outlined by a red curve. (c) Conductance of the sample at $B = 0 \text{ T}$, $T = 1.7 \text{ K}$. Four regions of different polarities are indicated. A zoom of the transconductance in the boxed region with a solid line is shown in Fig. 2. The dashed (dotted) box indicates the gate voltage range in which Figs. 3a,b (d,e) were measured.

It should be noted that Eq. (1) can be used to describe the oscillations in all six samples, regardless of the number of graphene layers and the sample width (see table I).

The oscillations persist in magnetic fields up to $B = 1 \text{ T}$ for sample A and the periodicity scales with $\Delta\nu$ for the entire magnetic field range. In higher magnetic fields the conductance is dominated by quantum Hall edge channels and takes on values below e^2/h in the nnp and pnp regimes, in agreement with observations by Amet et al.⁹

The oscillatory conductance is quite robust against temperature changes. Figure 4a,b show the decay of the amplitude as a function of temperature T . The oscillatory conductance in the pnp and nnp regime disappear at

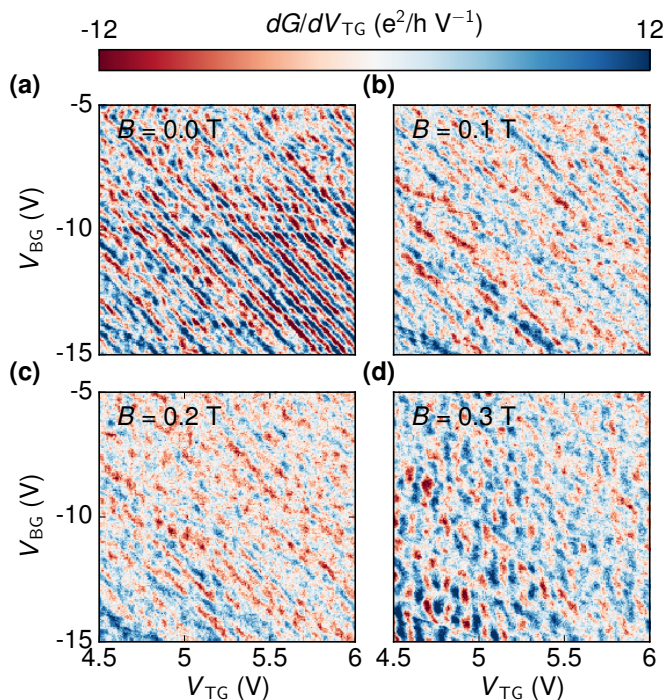


FIG. 2. Disappearance of Fabry-Pérot oscillations with increasing magnetic field. The measurement was taken in the boxed region with solid lines in Fig. 1c. At $B = 0$ T (a) the transconductance shows clear Fabry-Pérot oscillations. They disappear in a magnetic field of $B \gtrsim 0.1$ T (b-d).

a temperature around 30 K. As can be seen in Fig. 4c, at $T = 10$ K the oscillations are still clearly present, while the Shubnikov-de Haas oscillations in the $pp'p$ regime have already faded out.

The above discussed oscillations can be reproduced by transport calculations for an ideal SLG p - n junction at an intermediate magnetic field B , based on the scalable tight-binding model¹⁵. The ideal junction is modeled by connecting two semi-infinite graphene ribbons (oriented along armchair) with their carrier densities given by n_L in the far left and n_R in the far right. A simple hyperbolic tangent function with smoothness 50 nm bridging n_L and n_R is considered; see the inset of Fig. 5a for an example. To cover the density range up to $\pm 3 \times 10^{12} \text{ cm}^{-2}$ corresponding to maximal Fermi energy of $E_{\text{max}} \approx 0.2$ eV, the scaling factor $s_f = 10$ is chosen because it fulfills the scaling criterion¹⁵ $s_f \ll 3t_0\pi/E_{\text{max}} \approx 141$ very well; here $t_0 \approx 3$ eV is the hopping energy of the unscaled graphene lattice. Note that the following simulations consider $W = 1 \mu\text{m}$ for the width of the graphene ribbon, but simulations based on a different width show an identical oscillation behavior (See Supporting Information for details), confirming its width-independent nature as already concluded from our measurements.

The transmission function $T(n_R, n_L)$ across the ideal p - n junction at $B = 0.5$ T is shown in Fig. 5a, where fine oscillations along symmetric bipolar axis (marked by the

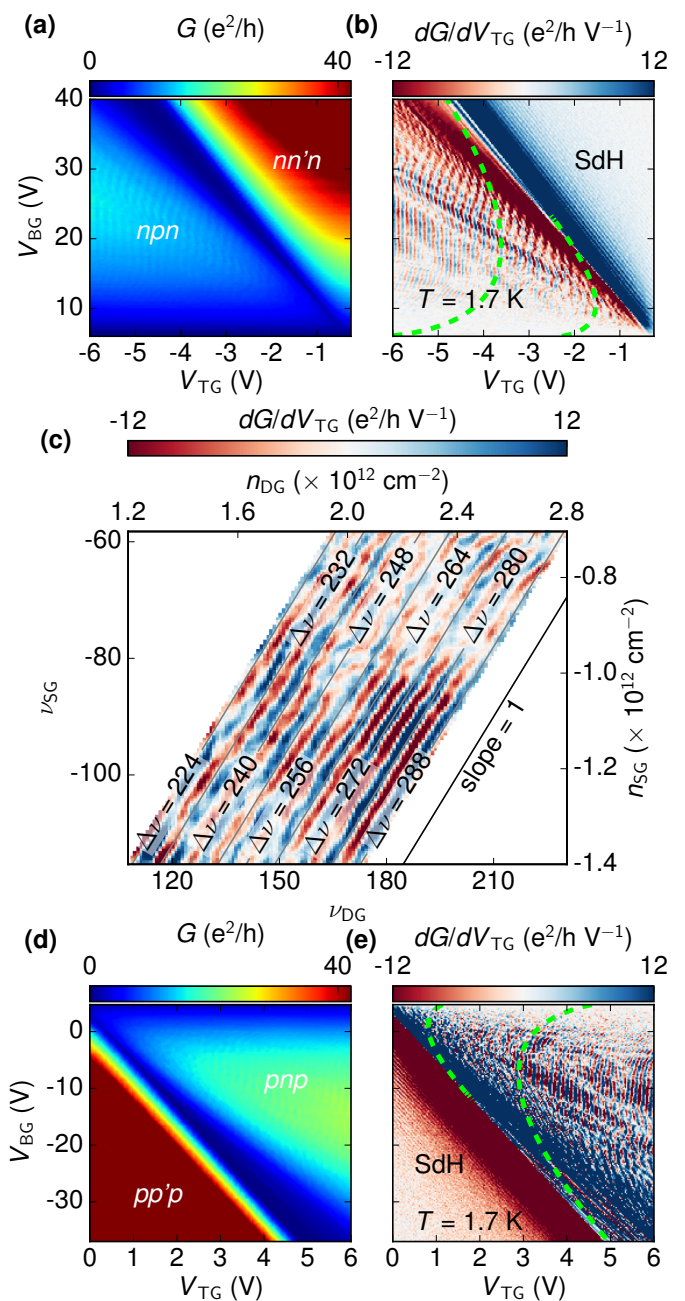


FIG. 3. Magnetotransport at $B = 0.5$ T. (a) Conductance of the sample at 0.5 T, showing an oscillatory pattern in the nnp regime. The measurement was taken in the dashed boxed region of Fig. 1c. (b) The oscillatory pattern in the nnp regime is more clearly visible in the transconductance. Green dashed lines indicate the pattern expected for snake states. In the $nn'n$ regime some faint lines can be distinguished, following the slope of the charge neutrality line of the dual gated region. These are Shubnikov-de Haas oscillations. (c) Transconductance at $B = 0.5$ T in the pnp regime as a function of charge carrier density (and filling factor) in the single- and dual-gated region. The oscillatory pattern follows the indicated line of slope one and can therefore be described by lines of constant filling factor difference $\Delta\nu = \nu_{\text{DG}} - \nu_{\text{SG}}$. (d),(e) Same as (a),(b), but with opposite charge carrier polarities. The oscillations are essentially particle-hole symmetric.

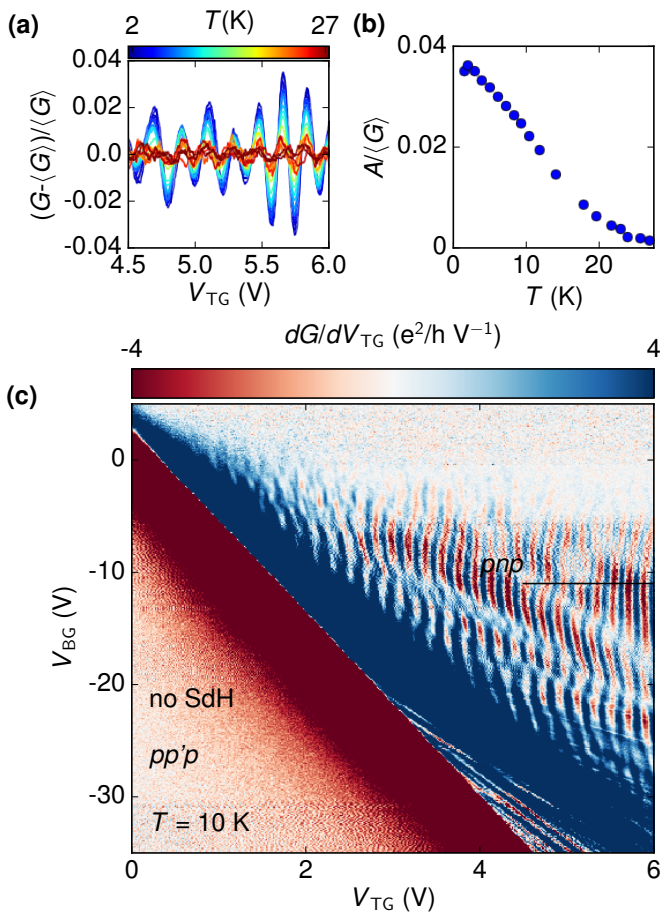


FIG. 4. Temperature dependence. (a) Oscillatory part of the conductance as a function of top gate voltage and temperature measured along the line cut indicated by the black line in Fig. 4c. (b) Amplitude A of the oscillatory conductance as a function of temperature. The oscillations disappear around $T = 30$ K. (c) Transconductance at $T = 10$ K, $B = 0.5$ T in the pn regime. Whereas Shubnikov-de Haas oscillations in the pp' regime have faded out, the oscillatory pattern in the pn regime persists.

blue arrows) from np to pn through the global charge neutrality point can be seen. Two regions marked by the white dashed boxes in Fig. 5a are zoomed-in and shown in Figs. 5b and d for a closer look and comparison with the measurements of sample B and E (Figs. 5c and e, respectively). Despite certain phase shifts (observed in Figs. 5b, d, and e) that are beyond the scope of the present study, good agreement between our transport simulation and experiment showing the oscillation period well fulfilling Eq. (1) can be seen.

Other works^{4,5} report on the formation of so called snake states along p - n interfaces in graphene. Snake states result in a minimum in the conductance whenever the sample width W and the cyclotron radius R_c satisfy $W/R_c = 4m - 1$ with m a positive integer. In the density range of Fig. 3b,e this would lead to two resonances at most (indicated by green dashed lines in Fig. 3b,e),

which is far less than the observed number of resonances. On top of that, snake states are inconsistent with the observed absence of a dependence on sample width. Furthermore, the tight-binding simulation also confirms that the observed effect is independent of the sample width and cannot be suppressed by introducing strong lattice defects in the vicinity of the p - n junction (see Supporting Information). We therefore rule out snaking trajectories as a possible cause of the observed oscillations.

Another process which could give rise to oscillations in a graphene p - n junction in a magnetic field is the interference of charge carriers which are partly reflected and partly transmitted at the interface. When the charge carrier densities are equal on both sides of the interface, electrons and holes will have equal cyclotron radii and therefore the paths of transmitted and reflected charge carriers will form closed loops. For the case of equal density, this model predicts the right periodicity of the oscillations.¹⁶ Experimentally, however, the measured oscillations are still visible when the densities on both sides of the p - n interface are quite different: at the point $(V_{BG}, V_{TG}) = (12, -6)$ V for example (see Fig. 3b), the cyclotron radii on the p and n side are respectively $0.36 \mu\text{m}$ and $0.16 \mu\text{m}$. The path lengths hence differ by $2\Delta R_c = 0.40 \mu\text{m}$, which is more than seven times the Fermi wavelength ($0.02 \mu\text{m}$ and $0.05 \mu\text{m}$). It seems unlikely that interference between charge carriers on skipping orbits can still occur in this density regime. On top of that, the tight-binding simulations show that the oscillatory pattern is still present when introducing large-area lattice defects in the vicinity of the p - n junction, which destroy the skipping trajectories (see Supporting Information). Thus the observed oscillations cannot be ascribed to interference of charge carriers on cyclotron orbits at the p - n interface.

Since the oscillations occur in both single-layer and bilayer graphene, we exclude an explanation that relies on specific details of the dispersion relation. In the magnetic field range where the oscillations are observed, the sample width is comparable to the classical cyclotron diameter. This excludes explanations based on classical electron flow following skipping orbit-like motion along edges.

A mechanism which may cause the oscillations involves the alignment of the density of states (DOS) around the Fermi energy. Diagrams of the DOS in the single- and dual-gated regions are sketched in Figs. 6a-c. Figure 6d shows a zoom in the map of the oscillatory transconductance of Fig. 3c. At point a in this zoom the filling factor in the dual-gated regime is $\nu_{DG} = 180$ and $\nu_{SG} = -92$ in the single-gated region. Because of the fourfold degeneracy of the Landau levels, Landau level numbers are $N = 45$ and $N = -23$ respectively, as shown in the DOS diagram of Fig. 6a. When following the oscillatory pattern from point a to point b, the two combs of DOS remain aligned with one another and only the Fermi level changes. This in contrast to what happens when moving from point a to point c: the DOSs shift with respect to one another and the transconductance oscil-

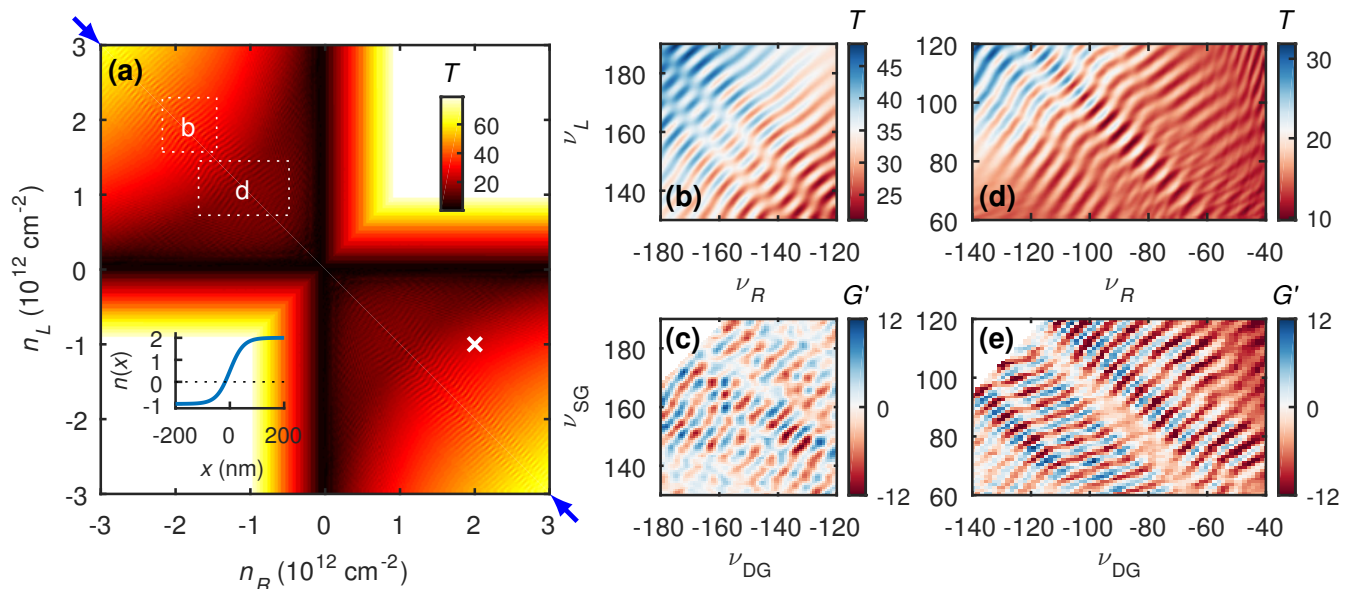


FIG. 5. (a) Transmission T as a function of the carrier densities in the left, n_L , and right, n_R , for an ideal SLG p - n junction at a perpendicular magnetic field $B = 0.5$ T based on a tight-binding transport calculation (color range restricted for clarity). Oscillations occur in the vicinity of the symmetric bipolar axis marked by blue arrows. Inset: an example of the considered carrier density profile corresponding to the white cross. White dashed boxes correspond to the density regions shown in panels (b) and (d), where the carrier density values are transformed in filling factors. (c)/(e) Transconductance G' measured for sample B/E shown with the filling factor range same as (b)/(d).

lates. It could therefore be the case that the alignment of the DOS affects the conductance of the p - n interface in a way similar to the magneto-intersubband oscillations (MISO) of a two-dimensional electron gas (2DEG):^{17,18} the occupation of two energy subbands of a 2DEG can lead to enhanced scattering between the subbands when the DOSs of the subbands are aligned. A similar enhancement of the coupling could occur in a graphene p - n junction. Just as for the oscillations we report on, MISO persist up to relatively high temperatures. The spacing predicted by this model lacks a factor of two compared to the experiment however: it would predict the argument of the cosine of Eq. (1) to be $2\pi\Delta\nu/4$. The explanation of the data requires the invocation of an even-odd asymmetry between the Landau levels to describe the measured periodicity: a coupling between Landau levels leading to higher/lower conductance when Landau levels of same/opposite parities are aligned, could account for the missing factor of two.

In conclusion, we have observed oscillations in the conductance of six graphene p - n junctions in the magnetic field range of $B = 0.4 - 1.5$ T. The oscillations are independent of sample width and can be described by the filling factor difference between the single- and dual-gated region. The oscillations are quite robust against temperature changes: they fade out only in the range of $T = 20 - 40$ K, whereas Shubnikov-de Haas oscillations decay below $T = 10$ K. The oscillations can be well reproduced by tight-binding transport calculations considering an ideal p - n junction at a constant magnetic field.

Up to a factor of two, the oscillatory pattern can be explained by considering the density of states alignment of the single- and dual-gated regions.

ACKNOWLEDGEMENT

We thank Péter Makk and François Peeters for fruitful discussions. We acknowledge financial support from the European Graphene Flagship and the Swiss National Science Foundation via NCCR Quantum Science and Technology. M.-H.L. and K.R. acknowledge financial support by the Deutsche Forschungsgemeinschaft within SFB 689.

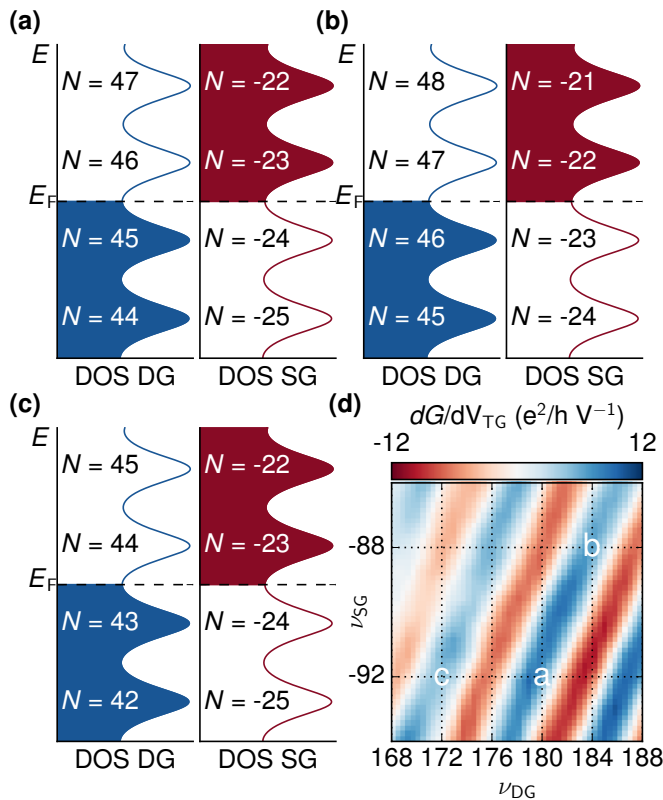


FIG. 6. (a-c) Schematics of the densities of states as a function of energy for the single- and dual-gated regions of the sample at positions a-c of the measurement (d) Zoom in Fig. 3c. The alignment of the densities of states can lead to an oscillatory pattern with the right slope: along the line from point a to point b the two combs of densities of states stay aligned, whereas the combs shift with respect to one another when moving from point a to point c.

- ¹ A. L. Grushina, D.-K. Ki, and A. F. Morpurgo, *Applied Physics Letters* **102**, 223102 (2013).
- ² P. Rickhaus, R. Maurand, M.-H. Liu, M. Weiss, K. Richter, and C. Schönberger, *Nature Communications* **4**, 2342 (2013).
- ³ A. Varlet, M.-H. Liu, V. Krueckl, D. Bischoff, P. Simonet, K. Watanabe, T. Taniguchi, K. Richter, K. Ensslin, and T. Ihn, *Physical Review Letters* **113**, 116601 (2014).
- ⁴ T. Taychatanapat, J. Y. Tan, Y. Yeo, K. Watanabe, T. Taniguchi, and B. Özyilmaz, *Nature Communications* **6**, 6093 (2015).
- ⁵ P. Rickhaus, P. Makk, M.-H. Liu, E. Tóvári, M. Weiss, R. Maurand, K. Richter, and C. Schönberger, *Nature Communications* **6**, 6470 (2015).
- ⁶ J. R. Williams, L. Dicarlo, and C. M. Marcus, *Science* **317**, 638 (2007).
- ⁷ B. Özyilmaz, P. Jarillo-Herrero, D. Efetov, D. A. Abanin, L. S. Levitov, and P. Kim, *Physical Review Letters* **99**, 2 (2007).
- ⁸ D. K. Ki, S. G. Nam, H. J. Lee, and B. Özyilmaz, *Physical Review B* **81**, 1 (2010).
- ⁹ F. Amet, J. R. Williams, K. Watanabe, T. Taniguchi, and D. Goldhaber-Gordon, *Physical Review Letters* **112**, 1 (2014).
- ¹⁰ E. Tóvári, P. Makk, P. Rickhaus, C. Schönberger, and S. Csonka, *Nanoscale* **8**, 11480 (2016).
- ¹¹ N. Kumada, F. D. Parmentier, H. Hibino, D. C. Glattli, and P. Roulleau, *Nature Communications* **6**, 8068 (2015).
- ¹² S. Matsuo, S. Takeshita, T. Tanaka, S. Nakaharai, K. Tsukagoshi, T. Moriyama, T. Ono, and K. Kobayashi, *Nature Communications* **6**, 8066 (2015).
- ¹³ C. R. Dean, A. F. Young, I. Meric, C. Lee, L. Wang, S. Sorgenfrei, K. Watanabe, T. Taniguchi, P. Kim, K. L. Shepard, and J. Hone, *Nature Nanotechnology* **5**, 722 (2010).
- ¹⁴ L. Wang, I. Meric, P. Y. Huang, Q. Gao, Y. Gao, H. Tran, T. Taniguchi, K. Watanabe, L. M. Campos, D. A. Muller,

- J. Guo, P. Kim, J. Hone, K. L. Shepard, and C. R. Dean, *Science* **342**, 614 (2013).
- ¹⁵ M.-H. Liu, P. Rickhaus, P. Makk, E. Tóvári, R. Maurand, F. Tkatschenko, M. Weiss, C. Schönenberger, and K. Richter, *Physical Review Letters* **114**, 1 (2015).
- ¹⁶ A. A. Patel, N. Davies, V. Cheianov, and V. I. Fal'ko, *Physical Review B* **86**, 1 (2012).
- ¹⁷ M. Raikh and T. Shahbazyan, *Physical Review B* **49**, 5531 (1994).
- ¹⁸ I. A. Dmitriev, A. D. Mirlin, D. G. Polyakov, and M. A. Zudov, *Reviews of Modern Physics* **84**, 1709 (2012).

Supporting Information for Oscillating Magnetoresistance in Graphene p-n Junctions at Intermediate Magnetic Fields

Hiske Overweg,¹ Hannah Eggimann,¹ Ming-Hao Liu,² Anastasia Varlet,¹ Marius Eich,¹ Pauline Simonet,¹ Yongjin Lee,¹ Kenji Watanabe,³ Takashi Taniguchi,³ Klaus Richter,² Vladimir I. Fal'ko,⁴ Klaus Ensslin,¹ and Thomas Ihn¹

¹*Solid State Physics Laboratory, ETH Zürich, CH-8093 Zürich, Switzerland*

²*Institut für Theoretische Physik, Universität Regensburg, D-93040 Regensburg, Germany*

³*Advanced Materials Laboratory, National Institute for Material Science, 1-1 Namiki, Tsukuba 305-0044, Japan*

⁴*National Graphene Institute, University of Manchester, Manchester M13 9PL, UK*

(Dated: December 20, 2016)

Overview

In the main text, we have shown a transmission map as a function of left and right carrier density, calculated using the real-space Green's function method based on the scalable tight-binding model [1]. The considered graphene ribbon of width $W = 1 \mu\text{m}$ is subject to a model density function describing an ideal pn junction with smoothness 50nm. The full map is repeated here in Fig. S1(a), with a white box marking the region plotted in Fig. S1(b).

In this Supporting Information, we show more numerical results in order to demonstrate that the observed oscillation is independent of the smoothness of the pn junction and the width of the graphene ribbon, and is not related the current along the pn junction. Instead, the oscillation is shown by the last numerical test to be closely related to the Landau levels away from the pn junction.

For quantitative and systematic comparisons, we will focus on the density range shown in Fig. S1(b) and the line cut on it along the dashed line shown in Fig. S1(c). All calculations shown in the following consider the same density range and resolution as Figs. S1(b) and (c), which can be regarded as the reference panels of this Supporting Information. In particular, the line cut of Fig. S1(c) will be repeatedly shown in the following results.

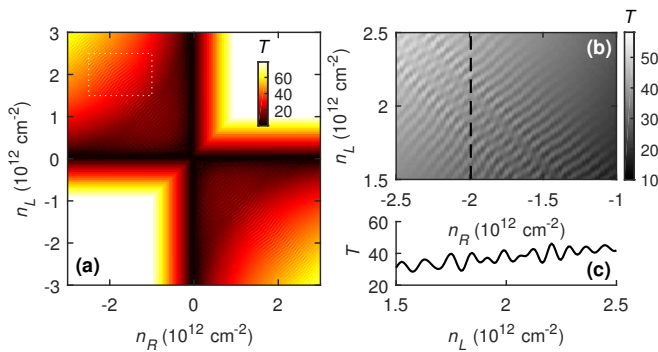


FIG. S1. (a) Transmission map $T(n_R, n_L)$ same as Fig. 5(a) in the main text (smoothness 50nm and graphene width $W = 1 \mu\text{m}$); white dashed box marks the region shown in (b), where a black dashed line indicates the line cut of $T(n_L)$ at fixed $n_R \approx -2 \times 10^{12} \text{cm}^{-2}$ shown in (c).

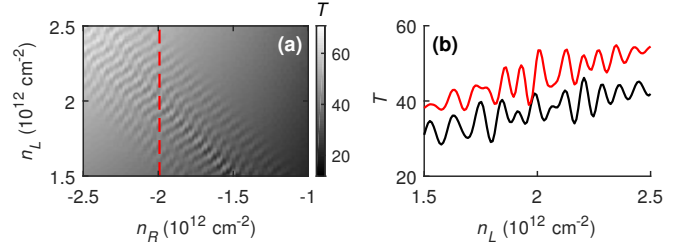


FIG. S2. (a) Transmission map $T(n_R, n_L)$ similar to Fig. S1(b) but with smoothness 25nm of the pn junction. The red dashed line indicates the line cut shown as a red line in (b), where the black line is the reference line identical to Fig. S1(c) for the case with smoothness 50nm.

Smoothness dependence

Figure S2(a) presents the transmission map with smoothness of 25nm, showing a similar pattern seen in Fig. S1(b) where the junction smoothness is 50nm. A more quantitative comparison is shown in Fig. S2(b) for the line cuts of the two cases. Despite a slightly higher T obtained for the sharper junction due to the Klein collimation [2], i.e., the sharper the pn junction, the wider the finite transmission probability of the angle distribution and hence the conductance, the general trend of the oscillation is shown to be independent of the smoothness.

In the rest of the numerical results, the smoothness will be fixed to 50nm.

Width dependence

Figure S3 presents the transmission map based on a graphene ribbon with $W = 0.9 \mu\text{m}$ shown in its panel (a) and $W = 0.8 \mu\text{m}$ shown in its panel (b). Comparing the line cuts in Fig. S3(c), along with the reference line of Fig. S1(c) for the case of $W = 1 \mu\text{m}$, the feature of the oscillation is clearly shown to be width-independent. On the other hand, the oscillation amplitude decreasing with the reduced graphene width implies that the oscillation may be closely related to the Landau levels in the bulk away from the pn junction, since the wider the graphene ribbon the better the Landau levels can develop.

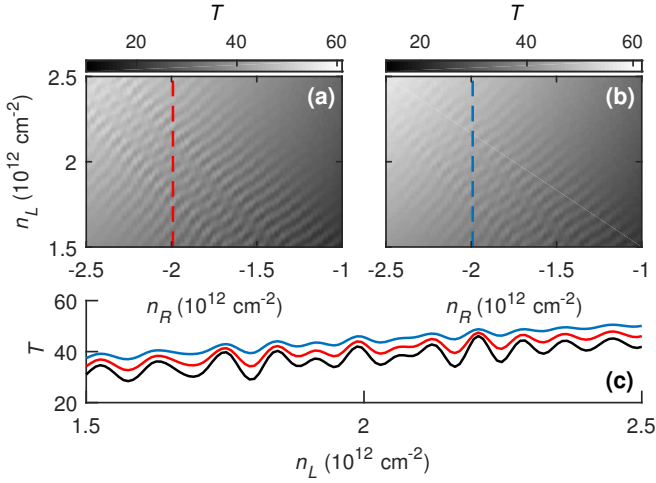


FIG. S3. Transmission maps $T(n_R, n_L)$ similar to Fig. S1(b) with the same smoothness of 50 nm but with (a) $W = 0.9 \mu\text{m}$ and (b) $W = 0.8 \mu\text{m}$. Line cuts along the red/blue dashed line marked in (a)/(b) are compared in (c) together with the reference line (black) of Fig. S1(c) for the case of $W = 1 \mu\text{m}$.

In the rest of the numerical results, the graphene width will be fixed as $W = 1 \mu\text{m}$.

Strong lattice defects

Next we show that the oscillation is not related to the current along the pn junction. To this end, we consider large-area lattice defects located in the vicinity of the pn junction. The basic idea is that if the oscillation came from any interference due to the current along the pn junction, such as the snake state [3], a large-area lattice defect at the pn interface or in the vicinity of it would act as a strong scatterer, destroying the interference and hence suppressing the oscillation. Contrarily, if the oscillation survives the introduced large defects, the current along the pn junction will then be ruled out from possible origins of the oscillation.

We first consider a $50 \times 400 \text{ nm}^2$ defect in Figs. S4(a) and (b); the defect is placed in front of the pn junction (at a distance 150 nm) in the former, and exactly on the pn junction in the latter. Despite an additional modulating pattern observed in Fig. S4(a), the fine oscillation patterns remain visible in both cases. By increasing the defect area to $300 \times 300 \text{ nm}^2$, the transmission map shown in Fig. S4(c) still exhibits the same oscillation pattern. A quantitative comparison of the line cuts summarized in Fig. S4(d) together with the reference line from Fig. S1(c) clearly shows that the oscillations observed in Figs. S4(a)–(c) belong to the same type as all those shown previously.

The fact that the strong defect introduced in the vicinity of the pn junction cannot suppress the oscillation clearly indicates that any possible interference effect due to the current along the pn junction cannot be the origin causing the oscillation. Instead, the oscillation seems to depend only on the Lan-

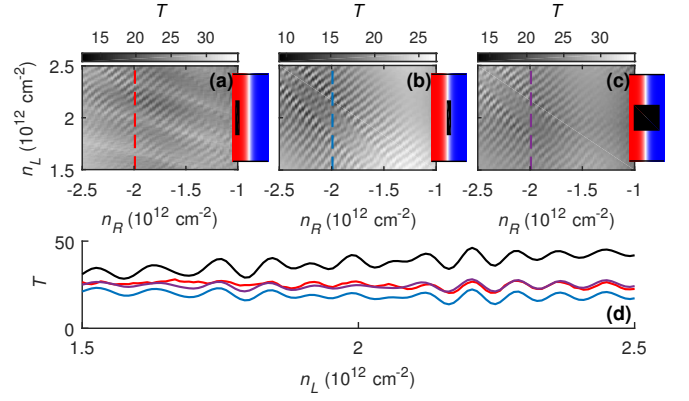


FIG. S4. (a)–(c) Transmission maps $T(n_R, n_L)$ similar to Fig. S1(b) with the same smoothness of 50 nm and width $W = 1 \mu\text{m}$, but with a large-area defect represented by the black rectangle shown in the individual inset to the right of each panel, where the color background depicts the y -independent model function $n(x, y)$ describing the density variation of the pn junction. The size of the defect is $50 \times 400 \text{ nm}^2$ in (a,b) and $300 \times 300 \text{ nm}^2$ in (c). Line cuts along the red/blue/purple dashed line marked in (a)/(b)/(c) are compared in (d) together with the reference line (black) of Fig. S1(c) for the case without the defect.

dau levels that are well developed in the semi-infinite leads.

Fixed leads

So far, all the presented calculations are based on an infinite graphene ribbon with a pn junction in the middle, as described in the main text. Technically, this is achieved in numerics by considering a scattering region of size $L \times W$ attached to two leads from the left and right, both floating with the density profiles at the attaching edge of the scattering region. As long as L is much longer than the smoothness of pn junction ($L = 400 \text{ nm}$ has been adopted in all the presented calculations), the density values at the left and right edges of the scattering region will saturate to a constant, and the entire open quantum system of the finite-size scattering region attached to the two floating semi-infinite leads will resemble an ideal pn junction in the middle of an infinitely long graphene ribbon, exhibiting an L -independent transmission behavior.

As a final and conclusive numerical test, we now fix the Fermi energies in the two semi-infinite leads at 0.1 eV, and consider the same range and parameters as the reference panel of Fig. S1(b). The calculated transmission map is shown in Fig. S5(a), which no longer exhibits the fine oscillation. The line cuts of fixed leads vs. floating leads compared in Fig. S5(b) clearly show that the oscillation completely vanishes in the present case of fixed leads.

The vanishing oscillation is consistent with what we have speculated from the previously shown tests that the oscillation originates from the resonance between Landau levels well developed in the far left and far right in the semi-infinite leads. The present case shown in Fig. S5 considers fixed Fermi ener-

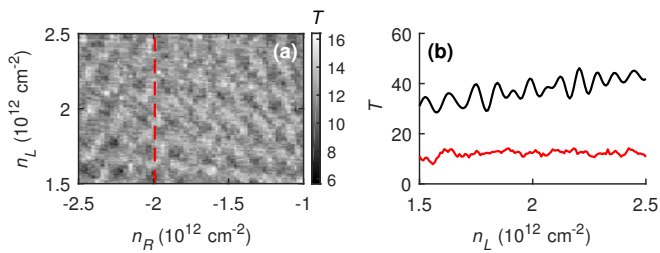


FIG. S5. (a) Transmission map $T(n_R, n_L)$ with the same range and parameters considered in Fig. S1(b) but with the two leads fixed at energy $E = 0.1$ eV. The red dashed line indicates the line cut shown as a red line in (b), where the black line is the reference line identical to Fig. S1(c) for the case with floating leads.

gies in the leads that no longer float with the densities n_R and n_L . Together with the fact that the length $L = 400$ nm $\ll W$ of the scattering region is too short for the Landau levels to form, the vanishing oscillation is therefore reasonably expected. By increasing the length of the scattering region to at least $L \approx W$, revival of the oscillation is expected for the case of fixed leads.

Note that the situation of fixed leads is actually closer to the

experiment, because the densities in graphene regions close to the contacts are rather pinned by the contact doping. However, the samples in our experiments (summarized in Table I in the main text) are long enough (several microns in all samples) for the Landau levels to develop well (with level spacing not far enough compared to disorder broadening in the magnetic field range we focus on) due to their cleanness and therefore exhibit the oscillation. Our numerical results based on floating leads correspond to the ideal case of infinitely long samples and therefore exhibit optimized oscillation.

-
- [1] M.-H. Liu, P. Rickhaus, P. Makk, E. Tóvári, R. Maurand, F. Tkatschenko, M. Weiss, C. Schönenberger, and K. Richter, *Phys. Rev. Lett.* **114**, 036601 (2015).
 - [2] V. V. Cheianov and V. I. Fal'ko, *Phys. Rev. B* **74**, 041403 (2006).
 - [3] P. Rickhaus, P. Makk, M.-H. Liu, E. Tóvári, M. Weiss, R. Maurand, K. Richter, and C. Schönenberger, *Nat. Commun.* **6**, 6470 (2015).